Journal of Magnetism and Magnetic Materials 503 (2020) 166615

Contents lists available at ScienceDirect

Journal of Magnetism and Magnetic Materials

journal homepage: www.elsevier.com/locate/jmmm

Research articles

Scale ratio modulated magnetic anisotropy of 3D $Ni_{1-x}Co_x$ crossed nanowire networks

Yenni G. Velázquez Galván[a], Tristan da Câmara Santa Clara Gomes[a], Luc Piraux[a], Joaquín de la Torre Medina[b,*]

[a] Institute of Condensed Matter and Nanosciences, Université catholique de Louvain, Place Croix du Sud 1, B-1348 Louvain-la-Neuve, Belgium
[b] Instituto de Investigaciones en Materiales – Unidad Morelia, Universidad Nacional Autónoma de México, Antigua Carretera a Pátzcuaro No, 8701 Col. Ex Hacienda de San José de la Huerta, C. P. 58190 Morelia, Mexico

ARTICLE INFO

Keywords:
Crossed nanowires
Ferromagnetic resonance
Magnetic anisotropy
NiCo alloys

ABSTRACT

In this work, three dimensional (3D) interconnected $Ni_{1-x}Co_x$ ($0 \leqslant x \leqslant 100\%$) crossed nanowire (CNW) networks with different scale ratios have been fabricated in order to investigate the influence of size reduction of the whole 3D networks structure on their crystal orientation and magnetic properties. Interconnected porous polycarbonate membranes, each one with different nanopore diameters but with the same porosity, have been designed to obtain porous architectures with different scale ratios. Using these membranes, CNW networks with the same packing fraction of about 22%, but different nanowires (NWs) diameters have been grown by electrodeposition. As a result, the magnetostatic (MS) anisotropy in the saturated state is the same for all the 3D networks, which allows identifying size dependent magnetic anisotropies. Reducing the diameter of the nanowires leads to changes on their magnetic properties, so that Co-rich CNW networks show a magnetocrystalline (MC) anisotropy contribution originated by a preferential hexagonal close packed orientation that competes with the MS anisotropy field. In turn, low diameter Ni-rich CNW networks show an anisotropy contribution of different nature than the MS and MC fields. The strategy presented in this work to accurately separate magnetic contributions leads to a better understanding of the magnetic behavior of complex 3D nanoarchitectures and to their potential use in the development of magnetic, sensing and spintronic applications.

1. Introduction

Novel nanomaterials based on 3D architectures are nowadays at the center of an extensive research activity due to their functional physical and chemical properties that make them very promising systems for a wide range of applications, like energy storage systems [1–3], catalysts [4,5], electronic sensors and actuators [6–8], biosensors [9] and complex-frustrated 3D nanostructured lattices [10]. Three dimensional networks made of CNWs have the potential for the development of novel multifunctional devices that exploit magnetic and microwave absorption properties [11,12], modulated magnetoresistive response [13,14] and spin-caloritronic behavior [15,16]. Particularly, 3D CNW networks are interesting materials for their application in technologies like magnetic filters [17–19], magnetic cell sorting [20,21] and 3D printing of materials [10,22–24]. NiCo alloys are very appealing ferromagnetic materials for all these technological applications because of their wide range of saturation magnetization values, maximum achievable anisotropic magnetoresistance ratio and large Seebeck coefficients and magnetothermopower values at room temperature [13,25,15]. As a consequence, understanding the fundamental magnetic behavior of NiCo CNW networks is one of the key aspects of the current scientific research in this area. Previous works on electrodeposited arrays of parallel NiCo NWs have reported on the expected transition between the fcc and hcp crystal orientations by varying the Co content [26] and its influence on the microstructure [27], microwave absorption [28] and magnetic properties like the coercive field and remanent magnetization [29,30], as well as on the magnetic anisotropy [31,32] and interaction and switching field distribution [33–35]. As known, interesting additional magnetic anisotropy contributions and effects appear as the diameter of the NWs is reduced [31,36,37], at the expense of giving rise to variations in the dipolar interaction field as a result of a change of the NWs packing fraction. Indeed, a central question for arrays of magnetic NWs is the accurate determination of individual magnetic anisotropy contributions when they are coupled to each other. Such a coupling may result from a simultaneous variation in the MC anisotropy and the dipolar interaction

* Corresponding author.
E-mail address: delatorre@iim.unam.mx (J. de la Torre Medina).

https://doi.org/10.1016/j.jmmm.2020.166615
Received 22 September 2019; Received in revised form 9 January 2020; Accepted 11 February 2020
Available online 12 February 2020

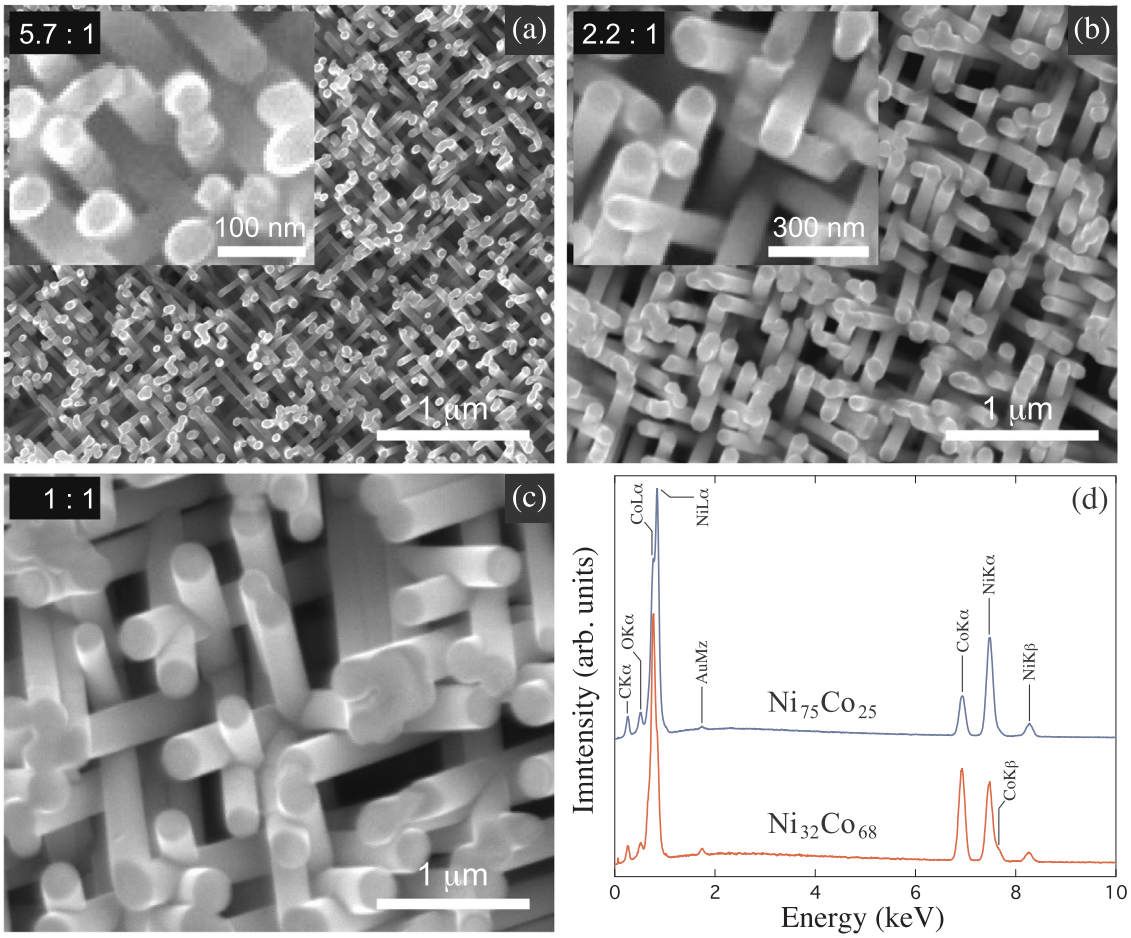

Fig. 1. Low magnification SEM micrographs of NiCo CNW networks with NW diameters of (a) 40 nm, (b) 105 nm and (c) 230 nm, obtained after the complete dissolution of the PC membrane. The scale bar corresponds to 1 μm. The insets in (a) and (b) display magnified sections of the same images by the respective scale ratios 230/40 ≈ 5.7 and 230/105 ≈ 2.2. (d) Measured energy-dispersive X-ray (EDX) spectra on $Ni_{76}Co_{24}$ and $Ni_{32}Co_{68}$ CNW networks with NWs diameter of 40 nm.

between NWs. One strategy to properly extract an anisotropy contribution is by keeping fixed the packing fraction between NWs at the same time their diameter is changed. This means that porous membranes must be designed in order to change the scale ratio of the resulting 3D networks that are expected to have the same packing fraction. In this work, this strategy has allowed to prepare CNWs with different scale ratios in order to subtract the MS field from the measured effective anisotropy field. As a result, excess anisotropy contributions which depend on the alloy composition and the NWs diameter have been determined with excellent accuracy. It is worth pointing out that the accurate determination of separate magnetic contributions of CNW networks is a step forward on the understanding of the magnetic behavior of complex 3D nanoarchitectures.

2. Materials and methods

Polycarbonate (PC) films of 20 μm thickness have been used to produce porous membranes with crossed nanopores by following a track etching process reported in a previous work, which consists in a sequential two-step exposure of energetic heavy ions at the angles ± 25° with respect to the normal of the PC films surface [14]. Next, the film was rotated in the azimuthal plane by 90° and re-exposed to the same irradiation flux to form finally a 3D interconnected nanochannel network. In both sequential irradiations the standard deviation was ± 5 degrees maximum around the target maximum angle. Three distinct as-prepared membranes with 3D interconnected nanopores with diameters of 40 nm, 105 nm and 230 nm were designed with an average volumetric porosity of approximately 22%. In order to keep constant this parameter for all the porous membranes, longer irradiation exposure times in the track etching process have been needed for PC membranes with lower nanopore diameters. The latent tracks were chemically etched in a 0.5 M NaOH aqueous solution at 70 °C to form nanopores with the desired diameters of 40 nm, 105 nm and 230 nm, following a previously reported protocol [38]. Later, using an e-beam evaporator, one side of the porous PC membranes were coated with a metallic Cr(10 nm)/Cu(150 nm) bilayer to serve as cathode for the electrochemical deposition.

Electrodeposition of CNW networks into porous PC templates has been done at room temperature in the potentiostatic mode using a Ag/AgCl reference electrode and a Pt counter electrode. Pure Ni CNW networks were grown at a constant potential of − 1.1 V using an electrolytic solution with concentration 1 M $NiSO_4$ + 0.5 M H_3BO_3 and the pH adjusted to 4, while pure Co CNW networks were grown at − 0.95 V using an electrolytic solution with concentration 1 M $CoSO_4{\cdot}7H_2O$ + 0.5 M H_3BO_3 and the pH adjusted to 5 by addition of NaOH. NiCo CNW networks were grown from two different electrolytes in order to obtain two distinct alloys. Alloyed $Ni_{76}Co_{24}$ and $Ni_{32}Co_{68}$ CNW networks were grown using the electrolytes with respective concentrations and reduction potentials of 1 M $NiSO_4{\cdot}6H_2O$ + 0.05 M $CoSO_4{\cdot}7H_2O$ + 0.5 M H_3BO_3 at − 1 V and 1 M $NiSO_4{\cdot}6H_2O$ + 0.2 M $CoSO_4{\cdot}7H_2O$ + 0.5 M H_3BO_3 at − 1 V. The pH of the as-prepared NiCo solution was lowered down to 2 by the addition of H_2SO_4.

For the morphological characterization of the 3D networks, first the Cr/Cu cathode was etched using a I2:KI (0.1:0.6 M) solution and then

the polycarbonate was dissolved with dichloromethane. The structural characterization has been carried out using a field-emission scanning electron microscope (FE-SEM). The magnetic properties were investigated by Alternating gradient Magnetometry (AGM-Lakeshore) and ferromagnetic resonance (FMR). Magnetization curves were obtained by AGM at room temperature in the out-of-plane (OOP) and in-plane (IP) directions of the CNW network plane, with a maximum applied field of ± 10 kOe. Besides, the FMR measurements were carried out in a microstrip line wave-guide configuration [11], which consists in a 500 μm wide and 500 nm thick microstrip evaporated on the free surface of the PC membranes after electrodeposition. Using this measurement setup has allowed to record room temperature FMR spectra by sweeping the magnetic field applied in the OOP direction from 10 kOe down to zero field, while keeping constant the excitation frequency in the range 40 MHz to 40 GHz. X-ray diffraction (XRD) experiments have been carried out by using a Bruker D2 Phaser X-ray diffractometer with a Cu radiation source of wavelength $\lambda = 1.54$ Å.

3. Results and discussion

Dissolution of the PC membrane was needed to carry out the structural characterization of the distinct 3D CNW networks. Fig. 1 shows SEM micrographs at the same magnification for CNW networks with nanowire diameters of (a) 40 nm, (b) 105 nm and (c) 230 nm. As seen, the three CNW networks show similar branching structure since the orientation and packing fraction of the NWs is the same. Indeed, the very similar packing fraction for all the three CNW networks is evident from the zoomed SEM micrographs, shown as insets in Fig. 1(a) and (b), at the respective scale ratios 230/40 ≈ 5.75 and 230/105 ≈ 2.2. In doing this, the zoomed NWs in the insets of Fig. 1(a) and (b) look as large and packed as those in Fig. 1(c). Besides, energy-dispersive X-ray (EDX) spectra do reveal changes for CNW networks of different compositions as shown in Fig. 1(d). As seen, the main differences between both spectra arise from emission lines CoLα, CoKα and CoKβ and NiLα, NiKα and NiKβ, which have larger intensity for respectively Co-rich and Ni-rich networks, as expected.

Further information about the crystal orientation of $Ni_{1-x}Co_x$ CNW networks has been obtained from XRD measurements. Typical XRD patterns for the lower and larger diameter Ni and Co CNW networks are shown in Fig. 2(a) and (b). XRD diffraction patterns for the 105 nm diameter CNWs are not shown for simplicity as they show an intermediate transition between those shown in these figures. All the XRD patterns have been normalized with respect to the more intense Ni or Co peak, so showing the relative intensity between them. For other elements the intensity of their peaks is meaningless as may appear larger than that for the Co and Ni peaks. For Ni CNWs, three peaks related to the fcc (1 1 1), fcc (2 0 0) and fcc (2 2 0) planes (COD 9008476) are observed for all CNWs diameters. In the case of Co CNWs, the XRD patterns show four peaks corresponding to the hcp (1 0 0), hcp (0 0 2), hcp (1 0 1) and hcp (2 1 0) planes (COD 9010967) for both NWs diameter. As the diameter of the NWs is changed, clear differences in the intensity of the XRD peaks are observed. The main difference is a larger relative intensity of the (0 0 2) peak for the low diameter NWs, whereas the opposite is observed for the larger diameter Co CNWs. Indeed, a different magnetic behavior is then expected for both CNW networks due to their distinct crystal orientations. Besides, low and large diameter $Ni_{76}Co_{24}$ CNW networks show similar XRD patterns to those for the Ni CNW networks, the main difference is the reduction of the relative intensity of the (2 0 0) peak. As the Co content increases to 68% two main features are observed from Fig. 2(a) and (b). First, the fcc Ni (1 1 1) and fcc Ni (2 2 0) peaks disappear at the expense of the hcp (0 0 2) and hcp (2 1 0) peaks. Second, mixed fcc and hcp phases are observed at this stage as the fcc Ni (2 0 0) peak and other Co planes like the hcp (1 0 0) and hcp (1 0 1) are detected together. Although the intensities of the hcp peaks for the Co CNW networks are significantly larger with respect to those for the Co-rich ones, their magnetic behavior is

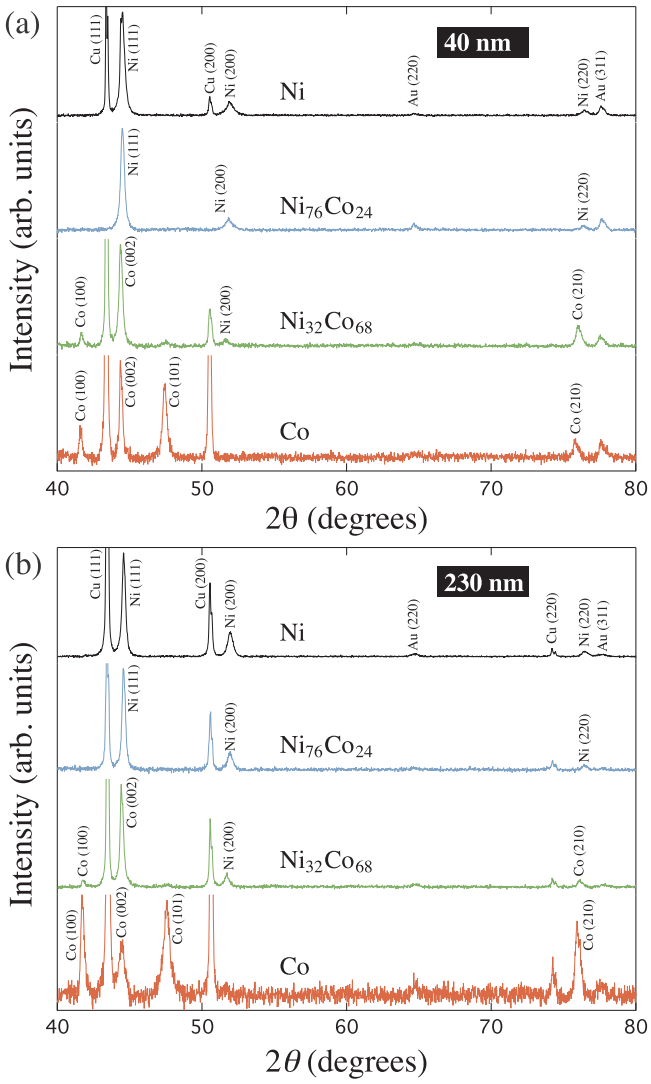

Fig. 2. X-ray diffraction patterns for $Ni_{1-x}Co_x$ CNW networks ($0 \leqslant x \leqslant 100\%$) with NW diameters of (a) 40 nm and (b) 230 nm.

expected to be similar as the Ni content is low. Besides, XRD peaks related to Cu (COD 9012954) and Au (COD 9008463), observed in almost all the XRD patterns, where detected from both the cathode used for the electrodeposition of the CNWs and the microstrip line used for the FMR experiments. Texture analysis has been carried out in order to determine the preferential crystallographic orientation of the CNW networks. To this end, the texture coefficient $TC(h\ k\ l)$ for the $(h\ k\ l)$ planes have been determined using the XRD patterns peak intensities along with the Harris formula [39]. Preferential $(h\ k\ l)$ texture is assumed when the corresponding texture coefficient is larger than one. Ni and Ni-rich CNWs are polycrystalline with barely preferential Ni(1 1 1) texture because in all cases $TC(1\ 1\ 1) \approx 1$. As the Co content increases to 68% mixed Co and Ni phases are observed in both XRD patterns. In this case, the preferential texture is clearly along the Co [0 0 2] direction with $TC(0\ 0\ 2)$ values of 2.26 and 3.40 for respectively the NWs diameter values of 40 nm and 230 nm. For the pure Co CNWs preferential (0 0 2) texture with $TC(0\ 0\ 2) = 1.8$ is only observed for $d = 40$ nm, whereas a preferential (2 1 0) texture with $TC(2\ 1\ 0) = 1.9$ is observed for $d = 230$ nm. Although the Harris formula gives a larger (2 1 0) texture for the largest diameter Co CNWs, the XRD pattern is quite similar those reported previously for large diameter Co NWs with preferential hcp Co(1 0 1) texture [40]. The interplay between the microstructural and magnetic properties is given later in the discussion

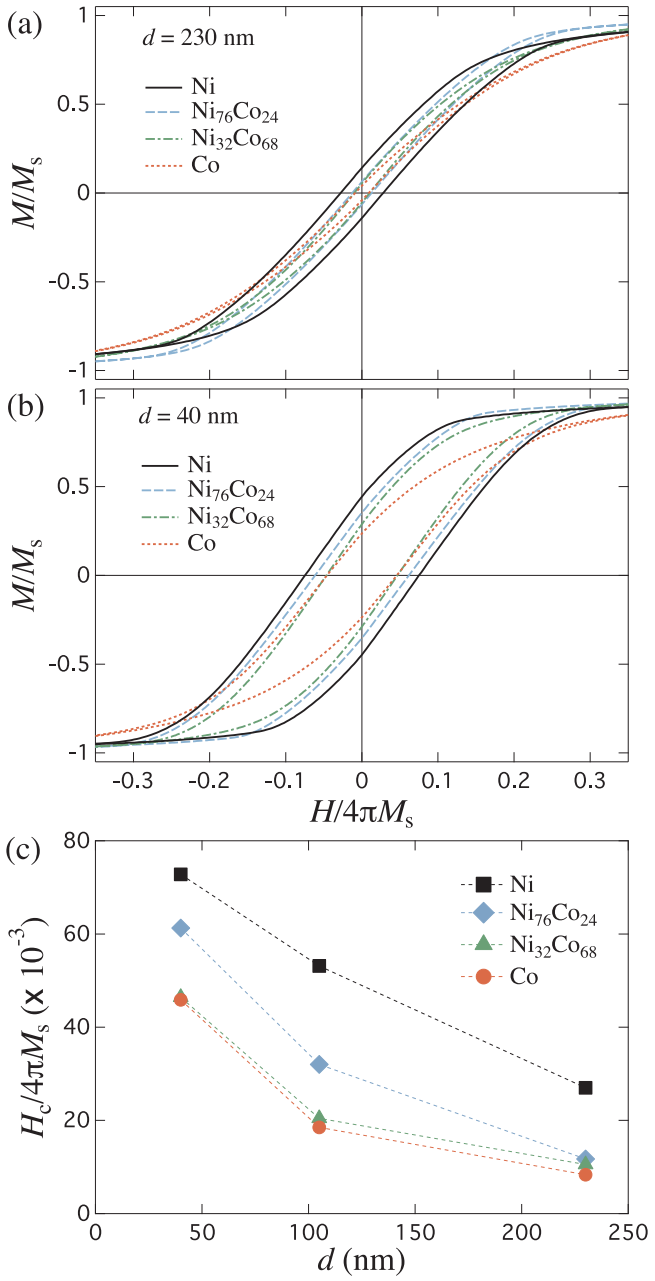

Fig. 3. Normalized hysteresis loops measured with the magnetic field applied along the OOP direction with respect to the plane of the PC membranes, in NiCo CNW networks with (a) the larger and (b) the lower NWs diameter. (c) Variation of the normalized coercive field as a function of the NWs diameter for the four series of NiCo CNW networks.

around Fig. 5.

The influence of the scale ratio and composition of CNW networks has been studied first by recording magnetization curves with the magnetic field applied in the OOP direction. Magnetic measurements are carried out along this direction because it is the magnetization easy axis of CNWs arranged at tilted angles close to the normal of the membrane plane, as shown in previous studies [11,13,14]. Fig. 3(a) and (b) show hysteresis loops for CNW networks with respectively the larger and the lower NWs diameter for the different Co contents. Hysteresis loops for the 105 nm diameter networks are not shown as they display an intermediate magnetic behavior. In both figures, the magnetization is plotted versus the dimensionless magnetic field which corresponds to the normalized applied field by the corresponding Co content dependent saturation magnetization ($M_s(x)$) value of each sample. The variation of M_s with the Co content x can be easily expressed by considering the linear variation of the saturation magnetization for NiCo alloys given by the Slater-Pauling curve [41], that is

$$M_s(x) = (1 - x)M_{Ni} + xM_{Co}, \quad (1)$$

where $M_{Ni} = 485$ emu·cm^{-3} and $M_{Co} = 1400$ emu·cm^{-3} are respectively the saturation magnetization values for Ni and Co. Since the effective anisotropy field is proportional to M_s, these normalized hysteresis loops only reveal the influence of magnetic anisotropy contributions different from the MS field. A common feature observed in both figures is the decrease of the hysteresis loops squareness and coercive field as both the NWs diameter and the Co content are increased. In one hand, the rapid decrease of the coercive field at larger NW diameters shown in Fig. 3(c) is consistent with the nucleation of magnetic domains. Indeed, these results are consistent with previous works on arrays of parallel Ni and Co NWs which have attributed the increase of the coercive field to the progressive crossover towards the single domain structure [42–46]. The case of pure Ni and Ni-rich CNWs is simpler than pure Co and Co-rich CNWs because the reduction of the coercive field is mediated only by the competition between shape anisotropy and the magnetic domain size that depends on the exchange stiffness constant, characteristic of each material [41]. On the other hand, lower values of the normalized coercive field $H_c/(4\pi M_s)$ take place at larger Co contents for a particular NWs diameter. Clearly, such a decrease is due to the hcp magneto-crystalline (MC) anisotropy of Co as it depends on the Co content. It has been shown in previous works that Co NWs are mainly single crystalline with the hcp c-axis perpendicular to their axis [11,47]. Such a crystal orientation is responsible of an additional MC anisotropy contribution that competes with the MS demagnetizing field. The larger shearing of the hysteresis loops for the Co CNW network suggests a lower effective magnetic anisotropy. Shearing of the hysteresis loop is associated to a decrease of the demagnetizing field because of the presence of dipolar interactions [48,49]. However, in this work the packing fraction of the CNW networks is almost the same, so the larger shearing of the Co hysteresis loops is due to the MC anisotropy contribution, showing that it works in a similar way in shaping the hysteresis loop.

In order to further investigate the influence of the CNW networks scale ratio on their magnetic behavior, FMR experiments in the field sweep mode with the magnetic field applied in the out-of-plane (OOP) direction, have been carried out. Fig. 4(a) and (b) show FMR spectra recorded at 20 GHz for CNW networks with NW diameters of 230 nm and 40 nm; measurements for the 105 nm diameter CNWs are not shown for simplicity since their behavior lies between those for the larger and the lower diameter CNWs. As seen in Fig. 4(a) for the case of the 230 nm diameter CNWs, the resonance field (H_r) at the minimum of the FMR spectra shifts towards lower field values as the Co content (x) is increased, which is consistent with the predicted variation of H_r with the increase of the saturation magnetization for NiCo alloys. The resonance condition, for an array of NWs tilted to a polar angle $\theta = 25°$ with respect to the applied field along the normal direction to the porous membrane plane, writes [14]

$$\left(\frac{f}{\gamma}\right)^2 = H_r^2 + A_1 H_{eff} H_r + A_2 H_{eff}^2, \quad (2)$$

where H_{eff} is the effective anisotropy field, $\gamma = 3.07$ GHz·kOe^{-1} is used here as the average gyromagnetic ratio for NiCo alloys and $A_1 = 1.464$ and $A_2 = 0.528$ are constants for $\theta = 25°$. The resonance condition of Eq. (2) can be solved for H_r in the case of purely magnetostatic systems by considering the effective anisotropy field H_{eff} is equal to the alloy composition dependent magnetostatic field

$$H_{ms}(x) = 2\pi M_s(x)(1 - 3P), \quad (3)$$

where $M_s(x)$ is given by Eq. (1) and P is the packing fraction of the CNWs. The calculated H_r values using Eqs. (1)–(3), indicated in

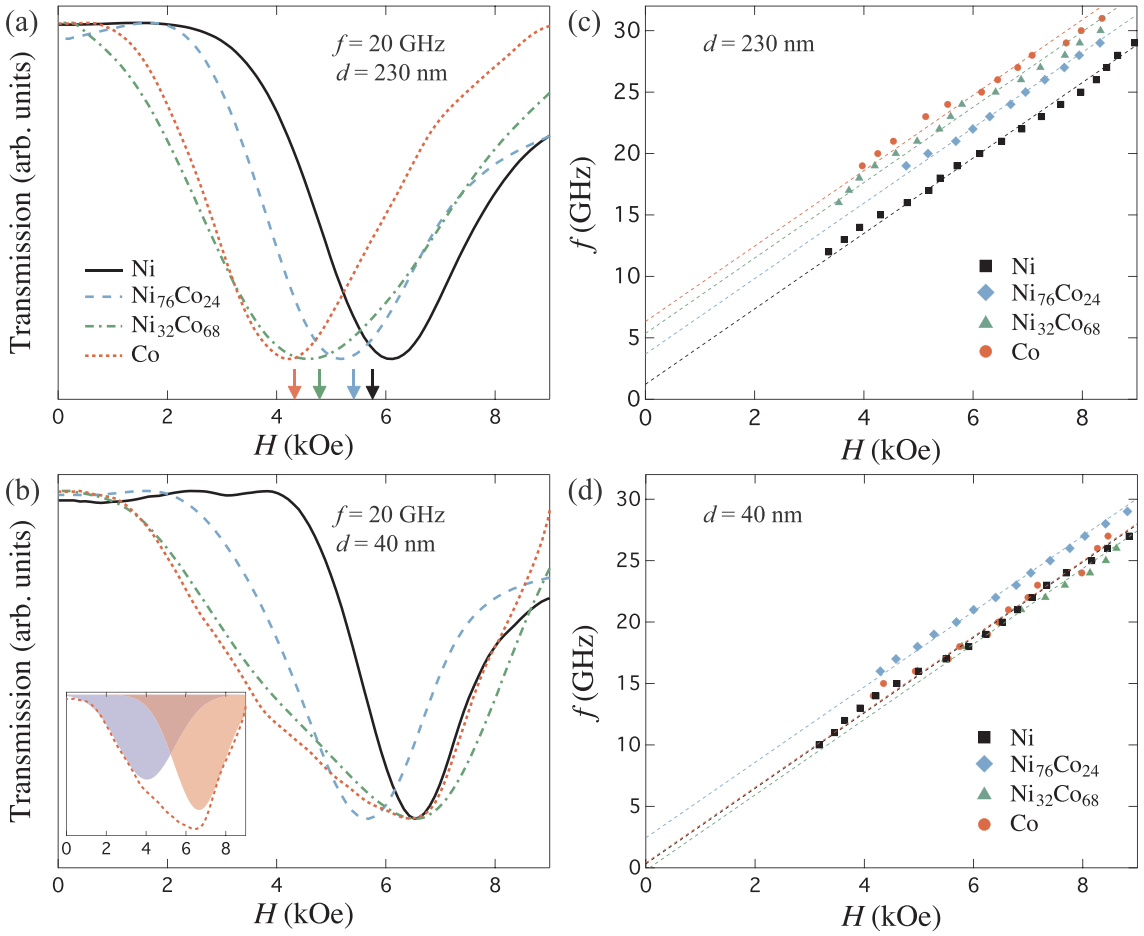

Fig. 4. FMR spectra recorded at 20 GHz on NiCo CNW networks with the same packing fraction and different NW diameters of (a) 230 nm and (b) 40 nm. The inset shows two gaussian distributions (shaded curves) used in the two peak fit of the FMR spectra for the pure Co CNWs (red dotted line). Dispersion relations for NiCo CNW networks with NW diameters of (c) 230 nm and (d) 40 nm. The dotted lines are fits to the dispersion relations using the resonance condition given by Eq. (2).

Fig. 4(a) by the vertical arrows of the same colors as those of the FMR spectra, are very close to their corresponding experimental resonance fields. This good agreement shows that the effective magnetic anisotropy of 230 nm diameter CNWs is dominated by the MS contribution. Conversely, the FMR spectra for the 40 nm diameter CNWs shown in Fig. 4(b) shifts back and forth with increasing the Co content, suggesting that other sources of magnetic anisotropy contribute to the overall behavior of these networks.

FMR spectra were recorded at other excitation frequencies in order to elucidate the difference between these behaviors. Fig. 4(c) and (d) show the excitation frequency vs. resonance field dispersion relations for the 230 nm and 40 nm diameter CNWs with different compositions. In one hand, the upward shift of the dispersion relation with increasing x for the 230 nm diameter CNWs observed in Fig. 4(c) is consistent with the resonance field shift towards lower values, as shown in Fig. 4(a). This means that dispersion relations located at higher frequencies provide larger anisotropy fields because of their corresponding larger $M_s(x)$. On the other hand, the dispersion relations for the 40 nm diameter CNWs also shifts back and forth with increasing the Co content, similarly to what is observed in Fig. 4(b), so no consistent monotonous variation of the resonance frequency as a function of $M_s(x)$ takes place.

A better insight on the magnetic behavior of these networks can be obtained from a careful analysis of the lineshape of the FMR spectra displayed in Fig. 4(b). As seen, at Co contents below 68% the FMR spectra are located almost at the same resonance fields and are as symmetrical as those for the larger diameter CNWs. As a result, the magnetic anisotropy for these alloys is mainly MS. At Co-contents higher than 68% H_r shifts back to higher fields, the FMR spectra are not symmetrical and display a shoulder located at lower resonance fields close to those expected for purely MS systems. As shown previously, FMR spectra recorded in the field sweep mode may be the result of the superposition of absorption peaks originated by distinct anisotropy contributions [36]. Therefore, for the pure Co CNW network the absorption at lower fields displayed as a shoulder in the spectrum (see Fig. 4(b)) is the result of a fcc-like Co fraction that contributes only to the MS field, whereas the main absorption located at higher fields is the result of an another magnetic anisotropy contribution. Indeed, low diameter pure Co NWs have a large hcp to fcc crystal orientations ratio [11,47], so in this case the lineshape of the absorption spectrum reflects a combination of both majority MC and minority MS anisotropies. A deeper insight on the FMR spectra lineshape can be obtained by following the procedure reported in a previous work used to identify the resonance fields of the main anisotropy contributions in the FMR spectra [36]. This procedure consists in reproducing broadened FMR spectra that clearly display two anisotropy contributions by using a two gaussian peak fit, as shown in the inset of Fig. 4(b) for the 40 nm diameter Co CNWs. In this figure, the minimum of the low field gaussian distribution (blue shaded area) is close to the resonance field due to the MS contribution (red vertical arrow in Fig. 4(a)), whereas the high field deeper gaussian distribution (red shaded area) explains the dominant hcp MC contribution for this network. Furthermore, since the absorption spectrum for the $Ni_{32}Co_{68}$ CNW network shows similar features as that for the pure Co CNW network, then its microstructure and magnetic behavior are expected to be very similar.

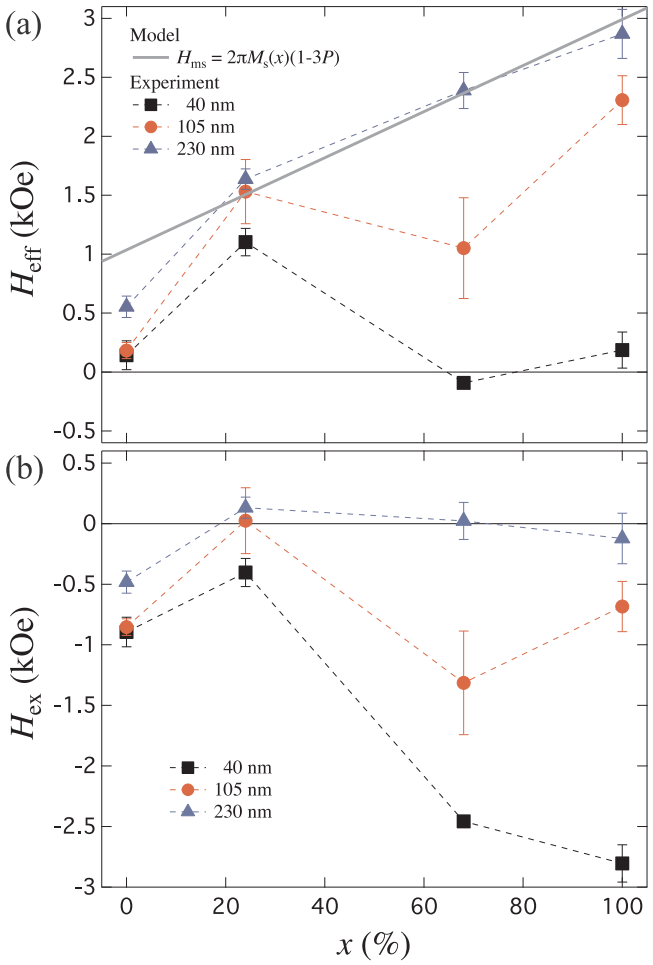

Fig. 5. Variation with the Co content x of (a) H_{eff} and (b) H_{ex} for $Ni_{1-x}Co_x$ CNW networks with different NW diameters. Error bars are the standard errors obtained from the fittings to the dispersion relations.

Quantitatively, the effective field can be obtained by fitting the resonance condition of Eq. (2) to the respective dispersion relation of each CNW network, as shown in Fig. 4(c) and (d) by the dotted lines. The resulting H_{eff} values are plotted in Fig. 5(a) as a function of the Co content, x, for the three NW diameters of 40 nm, 105, nm and 230 nm. For most of the CNW networks $H_{eff} > 0$, corroborating the fact that the OOP direction is the easy axis of magnetization. As seen, H_{eff} increases monotonically with x for the case of the 230 nm diameter CNWs, in good agreement with the expected variation of the MS field given by Eq. (3) (continuous grey line) and with previous results reported for parallel NiCo NWs [28]. The packing fraction P in Eq. (3) corresponds to the membrane average volumetric porosity of about 22% for all the CNW networks, so increasing (decreasing) this parameter has the effect of shifting downwards (upwards) the entire variation of H_{eff} vs x. This parameter is independent on the NWs diameter and is associated to the dipolar interaction field $6\pi M_s P$ of the entire array, which directly competes with the self demagnetizing field $2\pi M_s$ of an isolated infinite cylinder [50]. Therefore, the importance of using relatively low values of $P < 1/3$ ensures $H_{eff} > 0$, that is, an alignment of the magnetization easy axis along the OOP direction. In this work the CNW networks scale ratio has been modified by changing the NWs diameter, but keeping P constant in order to ensure the same dipolar interaction in the saturated state with the aim of obtaining size dependent magnetic anisotropy contributions. Reducing the diameter of the NWs to 105 nm leads to a decrease of H_{eff} with respect to the expected linear variation of H_{ms} with x. Clearly, a larger decrease of H_{eff} takes place at larger x, which is consistent with the presence of an additional anisotropy contribution that increases with the amount of Co and competes with the MS field. For this intermediate diameter H_{eff} still increases with x, however, such a variation is not monotonous because the amount of hcp and fcc crystallites in the NWs may vary or be similar from one sample to the other. This increasing variation of H_{eff} is consistent with previously results on parallel NiCo NWs with intermediate diameters [31]. A further decrease of the CNWs diameter down to 40 nm leads to a larger decrease of H_{eff} for Co-rich alloys. These 3D networks are magnetically isotropic since the effective field is close to zero, suggesting the presence of strong competing anisotropies of distinct origins that cancel each other. Besides, all the pure Ni CNW networks have effective fields lower than the expected MS field value $H_{ms} = 1.04$ kOe. The larger difference between both fields is about 0.9 kOe for the 40 nm diameter CNWs. As known, the room temperature first order MC anisotropy constant of Ni of -0.5×10^5 erg·cm^{-3} leads to a MC field of about -100 Oe [41]. Such a low value do not fully explains the observed decrease in H_{eff} for the lower diameter Ni CNWs, so another source of magnetic anisotropy has to be considered. Indeed, it has been shown that a magnetoelastic (ME) anisotropy contribution can be induced in Ni NWs as a result of spatial confinement of their structure [36]. This means that for low diameter Ni CNWs such a contribution may be induced by residual stresses at specific regions of the 3D networks, as for instance at the crossing zones between NWs. Similarly to the large positive magnetic anisotropy enhancement of ME origin observed in alumina membranes based arrays of Ni NWs [36], arrays of low diameter Ni NWs in PC membranes exhibit a negative anisotropy contribution which is likely of the same origin and competes with the shape anisotropy, so reducing the effective anisotropy field of the arrays [51]. A general additional excess anisotropy field (H_{ex}) is assumed in order to take into account these magnetic contributions. Consider then the effective field as the superposition of the MS contribution and this additional field, that is

$$H_{eff} = H_{ms} + H_{ex}, \quad (4)$$

where H_{ms} is given by Eq. (3) and is shown in Fig. 5 (a). Combining Eqs. (3) and (4) along with the experimental effective fields lead the excess fields for all CNW networks, as shown in Fig. 5 (b). As expected, this field is close to zero for the case of the 230 nm diameter CNWs because the magnetic behavior is dominated by the MS contribution.

Conversely, H_{ex} is non negligible and negative for most CNW networks with NW diameter values lower than 230 nm, the exception is the alloy composition with $x = 0.24$ for whatever diameter of the NWs. For this particular alloy the excess field is zero, consistent with its negligible MC anisotropy [26]. As discussed previously, the excess field for pure Ni CNWs can be explained in terms of a combination of their MC anisotropy and ME effects. For alloy compositions with $x \geqslant 0.24$ the increase of $|H_{ex}|$ with x is consistent with the increase of the hcp to fcc crystal orientations ratio. The fact that H_{ex} is larger for a particular x as the diameter of the NWs decreases is the consequence of an improvement of the hcp crystal texture which is naturally related to larger MC fields. Specifically, the hcp Co texture parameter $TC(0\ 0\ 2)$ is larger at lower diameters for pure Co CNWs, so a strong Co(0 0 2) texture indicates a reinforcement of the crystallographic hcp c-axis and consequently a larger MC anisotropy contribution. Indeed, this feature is consistent with previous observations on the interplay between the NWs diameter and crystal quality, as in parallel Co NWs [45,44] and Ni NWs [52,36]. Besides, $Ni_{32}Co_{68}$ CNW networks also have a strong Co(0 0 2) texture with even larger texture parameter than pure Co CNW networks which, on the contrary, increases as the diameter of the NWs is increased. Therefore, one might expect even larger MC fields for large diameter CNWs. However, the results in Fig. 5 (b) show the opposite behavior since H_{ex} decreases with increasing the NWs diameter. This discrepancy can be explained by the presence of Ni(2 0 0) planes with more intense diffraction peaks for larger CNWs diameters, as seen in Fig. 2. That is, a larger amount of Ni(2 0 0) in mixed Co and Ni

crystalline phases leads to a higher inhibition of the hcp MC anisotropy, as for CNWs with the largest diameter. The importance of the results discussed in this work lie on the fact that despite the complex spatial arrangement of 3D NiCo CNW networks and interconnections between NWs, their magnetic behavior remain sensitive to the alloy composition, crystal orientation and mechanisms that depend on size reduction and spatial confinement of the structure. Furthermore, interconnected 3D CNW networks are interesting materials with tunable magnetic behavior and robust mechanical properties which make them suitable for a wide variety of technological applications that require composite or free standing systems.

4. Conclusions

The variation of spatial parameters of 2D arrays of NWs or 3D networks of CNWs like the NWs diameter leads to changes in other parameters like the packing fraction of the entire systems. This leads to variations in distinct anisotropy fields at the same time, so decoupling them may be a difficult task. In this work we have proposed a methodology to extract specific magnetic anisotropy field contributions by decoupling them from the demagnetizing or magnetostatic field in large scale 3D CNW networks. To this end, interconnected porous membranes with the same porosity but specific NW diameters, have been prepared. This strategy has allowed to obtain CNWs with distinct scale ratios, that is, with the same packing fraction but allowing variations in the NWs diameter. Then, the MS field has been easily subtracted from the measured effective anisotropy field. Following this procedure, an excess anisotropy contribution that depends on the crystal orientation and the lateral dimensions of the NWs has been determined with remarkable accuracy. This field is of MC origin for Co-rich CNW networks, whereas it is negligible regardless the diameter of the NWs for the particular alloy composition with $x = 0.24$. In the case of pure Ni CNWs the excess field is consistent with a combination of MC and ME effects, where the last one may be originated by residual stresses resulted from the spatial confinement of the NWs. In short, NiCo CNW networks are very interesting 3D magnetic systems because their magnetic properties have been proven to be clearly detectable despite of their complex spatial arrangement and the amount of interconnections between NWs. Understanding the magnetic properties of these materials is paramount for the development of potential technological applications with 3D resolution, improved mechanical and large scale production capabilities.

Declaration of Competing Interest

The authors declare that they have no known competing financial interests or personal relationships that could have appeared to influence the work reported in this paper.

CRediT authorship contribution statement

Yenni G. Velázquez Galván: Methodology, Investigation, Validation, Data curation. **Tristan da Câmara Santa Clara Gomes:** Investigation, Resources, Validation. **Luc Piraux:** Supervision, Writing - review & editing, Funding acquisition. **Joaquín de la Torre Medina:** Conceptualization, Funding acquisition, Formal analysis, Writing - original draft.

Acknowledgements

The authors thank Dr. E. Ferain and the it4ip Company for supplying polycarbonate membranes. This work was partly supported by the Fédération Wallonie-Bruxelles (ARC 18/23–093 MICROBAT) and the 2019 UNAM-PAPIIT Program project IN106619. The work of Y. Velázquez-Galván was also supported by the Fonds de la Recherche Scientifique – FNRS and Fondo CONACYT - Secretaría de Energía - Hidrocarburos. T. da Câmara Santa Clara Gomes is a research fellow of the FNRS.

References

[1] Joel Ojonugwa Omale, Rico Rupp, Pascal Van Velthem, Vivien Van Kerckhoven, Vlad-Andrei Antohe, Alexandru Vlad, Luc Piraux, Three-dimensional micro-supercapacitors based on interdigitated patterns of interconnected nanowire networks, Energy Storage Mater. (2019).

[2] Tim Boettcher, Sandra Schaefer, Markus Antoni, Tobias Stohr, Ulrike Kunz, Michael Dürrschnabel, Leopoldo Molina-Luna, Wolfgang Ensinger, Falk Muench, Shape-selective electroless plating within expanding template pores: etching-assisted deposition of spiky nickel nanotube networks, Langmuir 35 (12) (03 2019) 4246–4253.

[3] Alexandru Vlad, Vlad-Andrei Antohe, Juan Manuel Martinez-Huerta, Etienne Ferain, Jean-François Gohy, Luc Piraux, Three-dimensional interconnected Ni_{core}–NiO_{shell} nanowire networks for lithium microbattery architectures, J. Mater. Chem. A 4 (2016) 1603–1607.

[4] Falk Muench, Metal nanotube/nanowire-based unsupported network electrocatalysts, Catalysts 8 (12) (2018).

[5] Qing Zhang, Xiao Lin Li, Bai Xiang Tao, Xiao Hu Wang, Yang Hui Deng, Xiao Ying Gu, Ling Jie Li, Wei Xiao, Nian Bing Li, Hong Qun Luo, CoNi based alloy/oxides@N-doped carbon core-shell dendrites as complementary water splitting electrocatalysts with significantly enhanced catalytic efficiency, Appl. Catal. B: Environ. 254 (2019) 634–646.

[6] Luc Piraux, Vlad-Andrei Antohe, Etienne Ferain, Driss Lahem, Self-supported three-dimensionally interconnected polypyrrole nanotubes and nanowires for highly sensitive chemiresistive gas sensing, RSC Adv. 6 (2016) 21808–21813.

[7] Meriem Akin, Autumn Pratt, Jennifer Blackburn, Andreas Dietzel, Paper-based magneto-resistive sensor: modeling, fabrication, characterization, and application, Sensors 18 (12) (2018).

[8] Kriti Agarwal, Sehyun Hwang, Aaron Bartnik, Nicholas Buchele, Avishek Mishra, Jeong-Hyun Cho, Small-scale biological and artificial multidimensional sensors for 3D sensing, Small 14 (35) (2018) 1801145 2019/05/29.

[9] Shuqi Wang, Xu. Li-Ping, Hai-Wei Liang, Yu. Shu-Hong, Yongqiang Wen, Shutao Wang, Xueji Zhang, Self-interconnecting Pt nanowire network electrode for electrochemical amperometric biosensor, Nanoscale 7 (2015) 11460–11467.

[10] Andrew May, Matthew Hunt, Arjen Van Den Berg, Alaa Hejazi, Sam Ladak, Realisation of a frustrated 3D magnetic nanowire lattice, Commun. Phys. 2 (1) (2019) 13.

[11] Tristan da Câmara Santa Clara Gomes, Joaquín de la Torre Medina, Yenni G. Velázquez-Galván, Juan Manuel Martínez Huerta, Armando Encinas, Luc Piraux, Interplay between the magnetic and magneto-transport properties of 3D interconnected nanowire networks, J. Appl. Phys. 120 (4) (2016) 043904.

[12] Mohanad K.I. Al Mamoori, Lukas Keller, Jonathan Pieper, Sven Barth, Robert Winkler, Harald Plank, Jens Müller, Michael Huth, Magnetic characterization of direct-write free-form building blocks for artificial magnetic 3D lattices, Materials 11 (2) (2018).

[13] Tristan da Câmara Santa Clara Gomes, Joaquín de la Torre Medina, Matthieu Lemaitre, Luc Piraux, Magnetic and magnetoresistive properties of 3D interconnected NiCo nanowire networks, Nanoscale Res. Lett. 11 (1) (2016) 466.

[14] Joaquín de la Torre Medina, Tristan da Câmara Santa Clara Gomes, Yenni G. Velázquez Galván, Luc Piraux, Large-scale 3-D interconnected Ni nanotube networks with controlled structural and magnetic properties, Sci. Reports 8 (1) (2018) 14555.

[15] Tristan da Câmara Santa Clara Gomes, Flavio Abreu Araujo, Luc Piraux, Making flexible spin caloritronic devices with interconnected nanowire networks, Sci. Adv. 5 (3) (03 2019) eaav2782.

[16] Flavio Abreu Araujo, Tristan da Câmara Santa Clara Gomes, Luc Piraux, Magnetic control of flexible thermoelectric devices based on macroscopic 3D interconnected nanowire networks, Adv. Electron. Mater. (2019) 1800819.

[17] Shehreen Aslam, Manoj Khanna, Veerakumar Veenugopal, Bijoy K. Kuanr, Microwave monolithic filter and phase shifter using magnetic nanostructures, AIP Adv. 8 (5) (2018) 056624 .

[18] R. Silvani, M. Kostylev, A.O. Adeyeye, G. Gubbiotti, Spin wave filtering and guiding in Permalloy/iron nanowires, J. Magn. Magn. Mater. 450 (2018) 51–59 Perspectives on magnon spintronics.

[19] R. Ramírez-Villegas, I. Huynen, L. Piraux, A. Encinas, J. De La Torre Medina, Configurable microwave filter for signal processing based on arrays of bistable magnetic nanowires, IEEE Trans. Microwave Theory Techniques 65 (1) (Jan 2017) 72–77.

[20] Daniel E. Shore, Thamotharampillai Dileepan, Jaime F. Modiano, Marc K. Jenkins, Bethanie J.H. Stadler, Enrichment and quantification of epitope-specific CD4+ T lymphocytes using ferromagnetic iron-gold and nickel nanowires, Sci. Reports 8 (1) (2018) 15696.

[21] Jiyun Lim, Mihye Choi, HyungJae Lee, Young-Ho Kim, Ji-Youn Han, Eun Sook Lee, Youngnam Cho, Direct isolation and characterization of circulating exosomes from biological samples using magnetic nanowires, J. Nanobiotechnol. 17 (1) (2019) 1.

[22] Eric MacDonald, Ryan Wicker, Multiprocess 3D printing for increasing component functionality, Science 353 (6307) (2016).

[23] Shuiren Liu, Xinlei Shi, Xiran Li, Yang Sun, Jian Zhu, Qibing Pei, Jiajie Liang, Yongsheng Chen, A general gelation strategy for 1D nanowires: dynamically stable functional gels for 3D printing flexible electronics, Nanoscale 10 (2018) 20096–20107.

[24] Tomke E. Glier, Lewis Akinsinde, Malwin Paufler, Ferdinand Otto, Maryam Hashemi, Lukas Grote, Lukas Daams, Gerd Neuber, Benjamin Grimm-Lebsanft, Florian Biebl, Dieter Rukser, Milena Lippmann, Wiebke Ohm, Matthias Schwartzkopf, Calvin J. Brett, Toru Matsuyama, Stephan V. Roth, Michael Rübhausen, Functional printing of conductive silver-nanowire photopolymer composites, Sci. Reports 9 (1) (2019) 6465.
[25] Tim Böhnert, Victor Vega, Ann-Kathrin Michel, Victor M. Prida, Kornelius Nielsch, Magneto-thermopower and magnetoresistance of single Co-Ni alloy nanowires, Appl. Phys. Lett. 103 (9) (2013) 092407 .
[26] T. McGuire, R. Potter, Anisotropic magnetoresistance in ferromagnetic 3d alloys, IEEE Trans. Magn. 11 (4) (1975) 1018–1038.
[27] S. Thongmee, H.L. Pang, J.B. Yi, J. Ding, J.Y. Lin, L.H. Van, Unique nanostructures in NiCo alloy nanowires, Acta Mater. 57 (8) (2009) 2482–2487.
[28] Y. Lei, L. Li, Tunable high-frequency properties of Co-Ni ferromagnetic nanowires through composition modulation. In 2015 IEEE International Magnetics Conference (INTERMAG), 2015, pp. 1–1.
[29] D.H. Qin, C.W. Wang, Q.Y. Sun, H.L. Li, The effects of annealing on the structure and magnetic properties of CoNi patterned nanowire arrays, Appl. Phys. A 74 (6) (Jun 2002) 761–765.
[30] A. Pereira, C. Gallardo, A.P. Espejo, J. Briones, L.G. Vivas, M. Vázquez, J.C. Denardin, J. Escrig, Tailoring the magnetic properties of ordered 50-nm-diameter coni nanowire arrays, J. Nanopart. Res. 15 (11) (Oct 2013) 2041.
[31] V. Vega, T. Böhnert, S. Martens, M. Waleczek, J.M. Montero-Moreno, D. Görlitz, V.M. Prida, K. Nielsch, Tuning the magnetic anisotropy of Co–Ni nanowires: comparison between single nanowires and nanowire arrays in hard-anodic aluminum oxide membranes, Nanotechnology 23 (46) (Oct 2012) 465709 .
[32] Miguel Méndez, Silvia González, Víctor Vega, Jose M. Teixeira, Blanca Hernando, Carlos Luna, Víctor M. Prida, Ni-Co alloy and multisegmented Ni/Co nanowire arrays modulated in composition: Structural characterization and magnetic properties, Crystals 7 (3) (2017).
[33] Javier García, Victor Vega, Lucia Iglesias, Victor M. Prida, Blanca Hernando, Enrique D. Barriga-Castro, Raquel Mendoza-Reséndez, Carlos Luna, Detlef Görlitz, Kornelius Nielsch, Template-assisted Co–Ni alloys and multisegmented nanowires with tuned magnetic anisotropy, Physica Status Solidi (a) 211 (5) (2014) 1041–1047.
[34] Philip Sergelius, Javier Garcia Fernandez, Stefan Martens, Michael Zocher, Tim Böhnert, Victor Vega Martinez, Victor Manuel de la Prida, Detlef Görlitz, Kornelius Nielsch, Statistical magnetometry on isolated NiCo nanowires and nanowire arrays: a comparative study, J. Phys. D: Appl. Phys. 49 (14) (Mar 2016) 145005 .
[35] A.S. Samardak, A.V. Ognev, A.Yu. Samardak, E.V. Stebliy, E.B. Modin, L.A. Chebotkevich, S.V. Komogortsev, A. Stancu, E. Panahi-Danaei, A. Fardi-Ilkhichy, F. Nasirpouri, Variation of magnetic anisotropy and temperature-dependent forc probing of compositionally tuned Co-Ni alloy nanowires, J. Alloy. Compd. 732 (2018) 683–693.
[36] J. de la Torre Medina, G. Hamoir, Y. Velázquez-Galván, S. Pouget, H. Okuno, L. Vila, A. Encinas, L. Piraux, Large magnetic anisotropy enhancement in size controlled Ni nanowires electrodeposited into nanoporous alumina templates, Nanotechnology 27 (14) (Feb 2016) 145702 .
[37] W.O. Rosa, L.G. Vivas, K.R. Pirota, A. Asenjo, M. Vázquez, Influence of aspect ratio and anisotropy distribution in ordered CoNi nanowire arrays, J. Magn. Magn. Mater. 324 (22) (2012) 3679–3682.
[38] E. Ferain, R. Legras, Track-etch templates designed for micro- and nanofabrication, Nucl. Instrum. Methods Phys. Res., Sect. B 208 (2003) 115–122 Ionizing Radiation and Polymers.
[39] G.B. Harris, X. quantitative measurement of preferred orientation in rolled uranium bars, The London, Edinburgh, and Dublin Philosophical Magazine and Journal of Science 43 (336) (1952) 113–123.
[40] A. Kazadi Mukenga Bantu, J. Rivas, G. Zaragoza, M.A. López-Quintela, M.C. Blanco, Structure and magnetic properties of electrodeposited cobalt nanowires, J. Appl. Phys. 89 (6) (2001) 3393–3397.
[41] B.D. Cullity, C.D. Graham, Introduction to Magnetic Materials, John Wiley & Sons Inc, second edition, 2009.
[42] A. Fert, L. Piraux, Magnetic nanowires, J. Magn. Magn. Mater. 200 (1) (1999) 338–358.
[43] J. Escrig, R. Lavín, J.L. Palma, J.C. Denardin, D. Altbir, A. Cortés, H. Gómez, Geometry dependence of coercivity in Ni nanowire arrays, Nanotechnology 19 (7) (2008) 075713 .
[44] Sirshendu Gayen, Milan K. Sanyal, Biswarup Satpati, Atikur Rahman, Diameter-dependent coercivity of cobalt nanowires, Appl. Phys. A 112 (3) (Sep 2013) 775–780.
[45] K. Maaz, S. Karim, M. Usman, A. Mumtaz, J. Liu, J.L. Duan, M. Maqbool, Effect of crystallographic texture on magnetic characteristics of cobalt nanowires, Nanoscale Res. Lett. 5 (7) (Apr 2010) 1111.
[46] Yu.P. Ivanov, M. Vázquez, O. Chubykalo-Fesenko, Magnetic reversal modes in cylindrical nanowires, J. Phys. D: Appl. Phys. 46 (48) (Nov 2013) 485001 .
[47] Michael Darques, Armando Encinas, Laurent Vila, Luc Piraux, Controlled changes in the microstructure and magnetic anisotropy in arrays of electrodeposited Co nanowires induced by the solution pH, J. Phys. D: Appl. Phys. 37 (10) (2004) 1411.
[48] H.J. Richter, The transition from longitudinal to perpendicular recording, J. Phys. D: Appl. Phys. 40 (9) (Apr 2007) R149–R177.
[49] J.M. Martínez Huerta, J. de la Torre Medina, L. Piraux, A. Encinas, Self consistent measurement and removal of the dipolar interaction field in magnetic particle assemblies and the determination of their intrinsic switching field distribution, J. Appl. Phys. 111 (8) (2012) 083914 .
[50] A. Encinas-Oropesa, M. Demand, L. Piraux, I. Huynen, U. Ebels, Dipolar interactions in arrays of nickel nanowires studied by ferromagnetic resonance, Phys. Rev. B 63 (Feb 2001) 104415 .
[51] Y. Velázquez-Galván, J. de la Torre Medina, L. Piraux, A. Encinas, Robustness of the enhanced magnetic anisotropy in Ni nanowires regardless of the deposition potential, J. Magn. Magn. Mater. 497 (2020) 165992 .
[52] S. Dellis, A. Christoulaki, N. Spiliopoulos, D.L. Anastassopoulos, A.A. Vradis, Electrochemical synthesis of large diameter monocrystalline nickel nanowires in porous alumina membranes, J. Appl. Phys. 114 (16) (2013) 164308 .